Sea-surface temperature patterns, radiative cooling, and hydrological sensitivity

Andrew I. L. Williams[1] **& Nadir Jeevanjee**[2]

[1]Program in Atmospheric and Oceanic Sciences, Princeton University
[2]Geophysical Fluid Dynamics Laboratory

Key Points:

- Hydrological sensitivity is systematically larger in uniform warming experiments compared to coupled experiments
- This is driven by larger increases in longwave, clear-sky radiative cooling under uniform warming
- These differences in longwave, clear-sky cooling arise due to different SST warming rates in regions of tropical deep convection

Corresponding author: Andrew Williams, andrew.williams@princeton.edu

Abstract

Global climate models project an increase in global-mean precipitation in response to increases in global-mean surface temperature; that is, a positive 'hydrological sensitivity'. Although linking global-mean precipitation to global-mean temperature is commonplace, there are hints in the literature that global-mean precipitation is sensitive to the *pattern* of warming in addition to global-mean warming. Here we show that hydrological sensitivity is about 25% larger in uniform warming scenarios compared to abrupt-4xCO_2 runs, a discrepancy on par with the inter-model spread in hydrological sensitivity under abrupt-4xCO_2 forcing. We link this discrepancy to changes in longwave, clear-sky radiative cooling in the tropics. We then build a simple theory which connects sea-surface temperature patterns to longwave, clear-sky cooling, and use this theory to quantitatively attribute these differences in hydrological sensitivity to differences in the rate of SST warming in regions of tropical convection.

Plain Language Summary

When climate scientists want to understand how the total amount of rainfall on Earth will change as the planet warms, they can use two types of computer simulations: one where ocean temperatures are warmed uniformly everywhere, and another where CO_2 is rapidly increased and the climate warms up in response. We show that the uniform warming experiments consistently predict about 25% more rainfall increase per degree of warming. The reason lies in where the warming occurs—uniform experiments heat up the rainy, stormy regions of the tropics just as much as everywhere else, while the natural response experiments tend to warm the dry Eastern tropical Pacific more than the rainy Western Pacific (similar to El Niño patterns). Since tropical thunderstorms are the atmosphere's main way of communicating temperature changes throughout the troposphere, warming the stormy regions more effectively 'stretches' the atmosphere and increases its ability to cool itself through radiation to space. To maintain energy balance, this enhanced cooling must be matched by more rainfall. This research helps explain why different experimental setups can give different predictions for future precipitation, and highlights that changes in the water cycle depend on not just how much warming occurs, but *where* that warming occurs.

1 Introduction

Since the earliest general circulation model (GCM) studies it has been noted that global-mean precipitation increases in response to increases in global-mean surface temperature (Manabe & Wetherald, 1975). Given this observation, it is common to define the 'hydrological sensitivity', η, which measures the rate of change of global-mean precipitation with respect to global-mean surface temperature. Global-mean precipitation is also affected by atmospheric 'adjustments' to climate forcers such as CO_2 or black carbon, but η just measures surface temperature-mediated component of global-mean precipitation change.

The reason for the increase in precipitation with surface warming is that, in the global-mean and in steady-state, latent heating of the atmosphere (through precipitation) must be balanced by atmospheric cooling, which is primarily achieved through longwave cooling to space (Methods) (Allen & Ingram, 2002; Pendergrass & Hartmann, 2014). To explain this increase in longwave cooling to space, Jeevanjee and Romps (2018) (hereafter, JR18) introduced a theory which relates changes in clear-sky radiative cooling to changes in the 'temperature depth' of the troposphere. We will revisit their argument in Section 5, but for now we note that the theory of JR18 provides a physical theory for what sets the order-of-magnitude of radiative cooling changes (and hence η) under warming.

While relating global-mean precipitation to global-mean temperature has been illuminating, there are a few cases in the literature which suggest η is sensitive to the *pattern* of SST warming in addition to its global-mean value. For example, Zhao and Knutson (2024) found that η was roughly 35% larger in atmosphere-only experiments where the imposed pattern of SST warming resembled the observed SST trend over recent decades compared to when the pattern was taken from the historical run of a coupled climate model. Similarly, S. Zhang et al. (2023) used 'patch warming' SST experiments with CAM5 to show that η was larger in response to SST warming in regions of tropical ascent compared to warming in other regions of the globe.

This potential dependence of η on SST patterns has also arisen in the context of different warming scenarios explored as part of the Coupled Model Intercomparison Project (CMIP). Specifically, in addition to the mandatory abrupt-4xCO_2 experiment in a fully-coupled model, many centers also ran uniform warming experiments with an atmosphere-only model. It is possible to calculate η using both of these setups (Fläschner et al., 2016), yielding two estimates of η. Interestingly, Fläschner et al. (2016) noted that, in the multi-model mean, η is *larger* when estimated using uncoupled, uniform-warming experiments than when estimated using fully-coupled abrupt-4xCO_2 simulations (see also Fig. 1a). We denote this difference between the η estimated using uniform warming simulations and abrupt-4xCO_2 simulations as

$$\Delta\eta \equiv \eta_{\text{uniform}} - \eta_{\text{abrupt}}. \tag{1}$$

The main difference between uniform warming and abrupt-4xCO_2 simulations is that abrupt-4xCO_2 simulations develop different sea-surface temperature (SST) warming *patterns*. For example, abrupt-4xCO_2 simulations tend to warm more in the Eastern tropical Pacific than the Western tropical Pacific (sometimes called an 'El Niño-like' warming pattern). So, could differences in SST warming patterns explain the difference between η_{uniform} and η_{uniform} across models? Fläschner et al. (2016) argue that patterned SST warming is *not* the reason for higher mean η in uniform warming simulations, because η estimated from AMIP-future4K simulations (which exhibit patterned SST warming) is similar to η_{uniform}. However, the warming pattern in AMIP-future4K simulations differs markedly from the abrupt4xCO2 warming trend in CMIP models (Qin et al., 2022; S. Zhang et al., 2023) and exhibits a tropical warming pattern which is in fact quite uniform (Voigt et al., 2024). Hence, the argument presented by Fläschner et al. (2016) does not rule out a role for patterned SST warming in driving a positive $\Delta\eta$.

In contrast to Fläschner et al. (2016), a recent paper by S. Zhang et al. (2023) argued that SST warming patterns were in fact a driver of the positive $\Delta\eta$ in models. Their methodology relies on using a linear Green's function from a single model (CAM5, (Zhou et al., 2017)) to reconstruct global-mean precipitation changes across the CMIP5 models. However, it is now well-established that Green's functions systematically fail to capture the behavior of abrupt-4xCO2 simulations (Dong et al., 2019; B. Zhang et al., 2023; Bloch-Johnson et al., 2024), casting doubt on the robustness of their results. For example, although it is not emphasized in their paper, the η reconstructed using CAM5 Green's functions is not significantly correlated to the η from individual CMIP5 models. Furthermore, although S. Zhang et al. (2023) point to the importance of warming in regions of tropical ascent, they do not provide a mechanism which links warming in such regions to changes in radiative cooling.

The literature thus raises a couple of questions: 'Does hydrological sensitivity depend on the pattern of SST warming?' and, if so, 'What mechanisms cause this?'. Furthermore, do these mechanisms arise from existing theories for hydrological sensitivity, or do they represent entirely different physics?

Give these questions, our goal in this paper is to quantify the link between SST patterns, radiative cooling, and η, with an eye towards explaining the positive $\Delta\eta$ across models in terms of their differing SST patterns. We begin by demonstrating that $\Delta\eta$ is in fact *systematically* positive across CMIP models, i.e. that every CMIP model has $\eta_{\text{uniform}} > \eta_{\text{abrupt}}$. We then decompose $\Delta\eta$ into contributions from changes in sensible heat fluxes and longwave/shortwave radiative cooling using the global-mean atmospheric energy budget (Eq. 2). We then build a theory (leveraging insights from Fueglistaler et al. (2015) and Jeevanjee and Romps (2018)) to *quantitatively* link changes in clear-sky radiative cooling to different patterns of SST warming. We conclude by arguing that the systematically positive $\Delta\eta$ across models is because uniform warming simulations have stronger warming in regions of tropical deep convection than abrupt-4xCO_2 simulations, leading to greater tropospheric deepening. We then discuss how our theory can explain recent results in the literature related to SST warming patterns and hydrological sensitivity.

2 Methods

2.1 CMIP simulations

We use an ensemble of simulations from the Coupled Model Intercomparison Project, Phases 5 & 6. We use all models for which all data was available for the abrupt-4xCO_2, AMIP and AMIP-p4K simulations. We used monthly mean data to calculate all quantities, but down-sampled all timeseries to yearly frequency before calculating regressions to minimize the influence of serial autocorrelation on our statistics.

We used 15 models in total, 8 from CMIP5 and 7 from CMIP6. We choose to combine CMIP5 and CMIP6 together throughout the paper to increase the sample size, but our conclusions are unchanged if we restrict ourselves to simply using a single generation of models. A full list of the models used is provided in the Supplement.

2.2 Global-mean energetic decomposition

Changes in precipitation with warming can be understood using the steady-state, global-mean atmospheric energy budget (Pendergrass & Hartmann, 2014). This states that the net heating of the atmosphere through latent heat release, shortwave absorption and surface sensible heat flux must be balanced by the longwave radiative cooling of the atmosphere (Mitchell et al., 1987; O'Gorman et al., 2012). When considering climate perturbations, denoted by δ, we can rearrange this balance to get an expression for changes in precipitation,

$$L\delta P = \delta Q_{\text{LW}} - \delta Q_{\text{SW}} - \delta\text{SHF}, \tag{2}$$

where L is the latent heat of condensation of water vapor, P is the precipitation rate, Q_{LW} is the longwave radiative cooling, Q_{SW} is the shortwave absorption and SHF is the upwards sensible heat flux at the surface (Methods).

We use Eq. 2 to understand the changes in global-mean precipitation in each of our experiments. We calculate the Q_{LW} and Q_{SW} terms in Eq. 2 as follows, with all terms positive in the direction indicated by their arrows:

$$Q_{\text{LW}} = \text{LW}^{\uparrow}_{TOA} + (\text{LW}^{\downarrow}_{SFC} - \text{LW}^{\uparrow}_{SFC}) \tag{3}$$

and

$$Q_{\text{SW}} = (\text{SW}^{\downarrow}_{TOA} - \text{SW}^{\uparrow}_{TOA}) + (\text{SW}^{\uparrow}_{SFC} - \text{SW}^{\downarrow}_{SFC}). \tag{4}$$

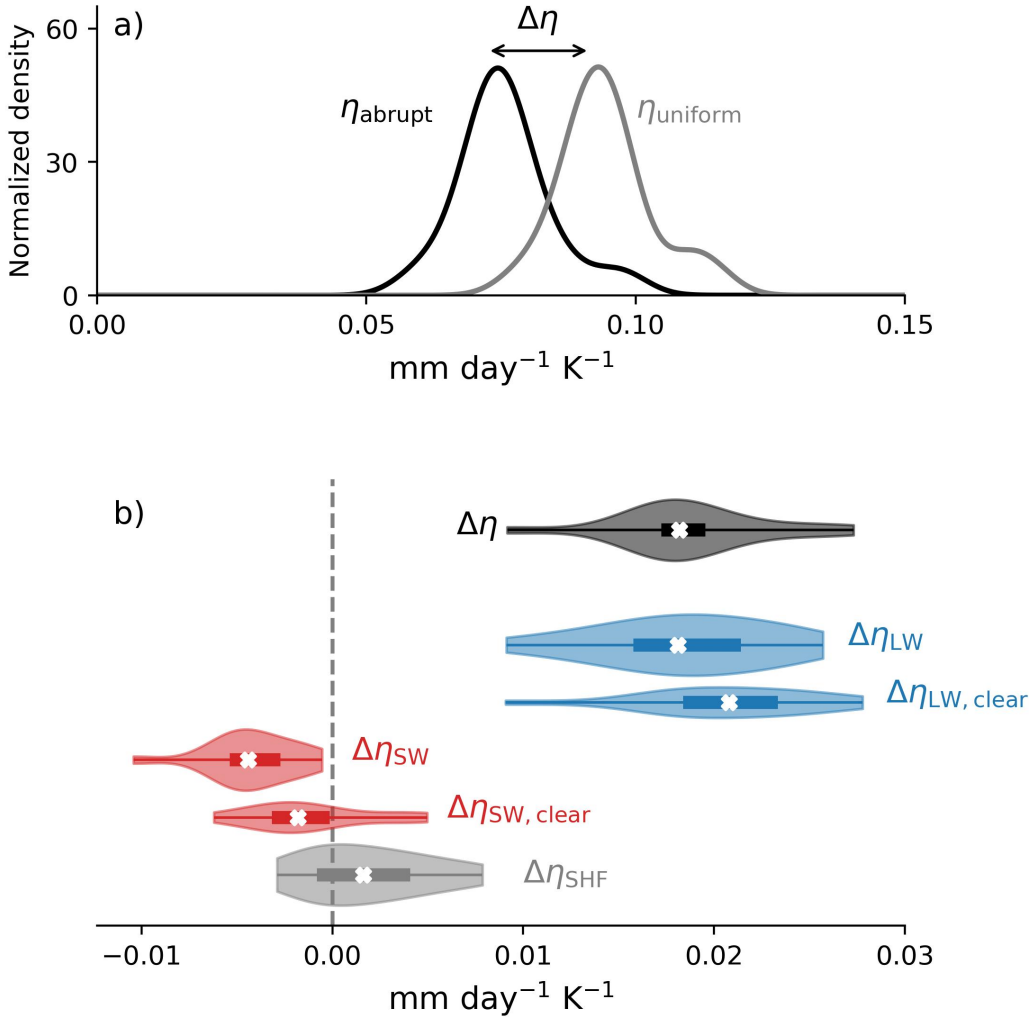

Figure 1. ***Hydrological sensitivity is systematically larger in uniform warming vs abrupt-4xCO$_2$ simulations, due to longwave clear-sky cooling.*** (a) Kernel density estimates of η calculated in uniform warming and abrupt-4xCO$_2$ simulations; kernel density estimates are computed using the `gaussian_kde` function from SciPy (Virtanen et al., 2020). (b) Violin plots of the difference in hydrological sensitivity ($\Delta\eta$) between uniform warming and abrupt-4xCO$_2$ simulations, with decomposition in contributions from longwave cooling ($\Delta\eta_{\text{LW}}$), shortwave absorption ($\Delta\eta_{\text{SW}}$) and sensible heat fluxes ($\Delta\eta_{\text{SHF}}$). Also shown are the contributions from clear-sky longwave cooling ($\Delta\eta_{\text{LW,clear}}$) and shortwave absorption ($\Delta\eta_{\text{SW,clear}}$). Distributions show the minimum and maximum changes; the median change plotted with a cross and the boxes show the inter-quartile range of changes.

All of the terms on the right-hand side of Eq. 2 are initially calculated in energy units (Wm^{-2}), before being transformed into 'precipitation units' (mm day^{-1}) for ease of presentation.

2.3 Hydrological sensitivity calculations

η measures the surface temperature-mediated component of global-mean precipitation change, and we estimate this in two ways. The difference between the AMIP-p4K and AMIP simulations is used to calculate η_{uniform}, and a regression approach is used to calculate η_{abrupt} in the abrupt-4xCO_2 simulations (Fläschner et al., 2016; DeAngelis et al., 2015). To estimate η_{abrupt}, we calculate a least-squares regression of global-mean precipitation against global-mean near-surface air temperature for years 0-140 of the abrupt-4xCO_2 scenario. Our conclusions are unchanged if we use the Theil-Sen estimator (which is more robust to outliers) instead of ordinary least squares regression.

Through the energy budget (Eq. 2), we can decompose hydrological sensitivity (η) into contributions from longwave cooling, shortwave absorption and sensible heat fluxes:

$$\eta = \eta_{\text{LW}} + \eta_{\text{SW}} + \eta_{\text{SHF}}. \tag{5}$$

Where we have absorbed the minus signs in the sensible heat flux and shortwave absorption terms from Eq. 2. For example, a positive η_{SHF} indicates a *reduction* in upwards surface sensible heat flux and a negative η_{SW} indicates an *increase* in shortwave absorption.

We calculate each of these terms by regression of their respective global-mean components against global-mean near-surface air temperature, as for η. We also decompose the longwave cooling and shortwave absorption terms into their clear-sky and cloudy-sky components.

3 Changes in η are driven by longwave, clear-sky cooling

We begin by demonstrating that η calculated using uniform warming simulations is in fact larger than η calculated from abrupt-4xCO_2 simulations, and that this is a common feature across models. This is a step beyond the results of Fläschner et al. (2016), who only showed that $\eta_{\text{uniform}} > \eta_{\text{abrupt}}$ holds in the multi-model mean.

Figure 1a shows probability density functions of η derived from both uniform warming and abrupt-4xCO_2 simulations. Visually, it is apparent that $\eta_{\text{uniform}} > \eta_{\text{abrupt}}$ in the multi-model mean. To assess whether this holds on a model-by-model basis, Figure 1b shows violin plots of the difference in η between uniform warming experiments and abrupt-4xCO_2 simulations (denoted as $\Delta\eta$). We find that η is systematically larger in uniform warming experiments compared to the abrupt-4xCO_2 coupled runs—i.e., a positive $\Delta\eta$—with a median difference of around $\Delta\eta \approx 0.02$ mm day^{-1} K^{-1}. In fractional terms, this means that η_{uniform} is on average about 25% larger than η_{abrupt} in CMIP models. This difference is comparable to the inter-model spread of η under abrupt-4xCO_2 forcing, further motivating its study.

In Figure 1b we also show the contributions to $\Delta\eta$ changes from longwave cooling ($\Delta\eta_{\text{LW}}$), shortwave absorption ($\Delta\eta_{\text{SW}}$) and upwards sensible heat fluxes at the surface ($\Delta\eta_{\text{SHF}}$). We also show the contribution from changes in clear-sky longwave cooling ($\Delta\eta_{\text{LW,clear}}$) and shortwave absorption ($\Delta\eta_{\text{SW,clear}}$). The larger hydrological sensitivity in uniform warming versus abrupt-4xCO_2 runs is mostly due to differences in clear-sky longwave cooling, while changes in sensible heat flux and clear-sky shortwave absorption are similar between the uniform warming and abrupt-4xCO_2 runs.

While $\Delta\eta_{\text{LW,clear}}$ captures the mean $\Delta\eta$ across models, inter-model spread in $\Delta\eta$ is not strongly correlated to inter-model spread in $\Delta\eta_{\text{LW,clear}}$, or indeed any of the energetic components (Supplementary Figure 1). Hence, in this paper our goal is to explain the *multi-model mean* of $\Delta\eta$ in terms of the *multi-model mean* of $\Delta\eta_{\text{LW,clear}}$. To achieve this, we will first link $\Delta\eta_{\text{LW,clear}}$ to changes in tropical radiative cooling, and then

link changes in tropical radiative cooling to the pattern of sea-surface temperature change. To make these links we will scatter results across models to demonstrate physical relationships, but the point is not to explain inter-model spread per se, but to demonstrate that we have a physical understanding of what sets $\Delta\eta_{\mathrm{LW,clear}}$.

4 Differences in $\Delta\eta_{\mathrm{LW,clear}}$ are driven by the tropics

We will now argue that $\Delta\eta_{\mathrm{LW,clear}}$ is primarily driven by *tropical* changes in longwave, clear-sky cooling per degree of global warming, as opposed to being associated with radiative changes in the extratropics. This is illustrated in Figure 2, which shows scatter plots of $\Delta\eta_{\mathrm{LW,clear}}$ against its contributions from tropical and extratropical radiative cooling. The tropical contribution to $\Delta\eta_{\mathrm{LW,clear}}$ is calculated as $\Delta\left(d\left\langle Q_{\mathrm{LW,clear}}\right\rangle/dT_s\right)$ where $\langle\cdot\rangle$ indicates a tropical average ($\pm30°$ of the equator), and Δ denotes the difference between a quantity calculated using uniform warming and abrupt-4xCO_2 experiments. The extratropical contribution is calculated similarly but we average the longwave, clear-sky cooling over all points poleward of $\pm30°$. Note that in order to keep things neat, in the bulk of the paper we will denote the tropical contribution to $\Delta\eta_{\mathrm{LW,clear}}$ as $\Delta\left\langle\eta_{\mathrm{LW,clear}}\right\rangle$.

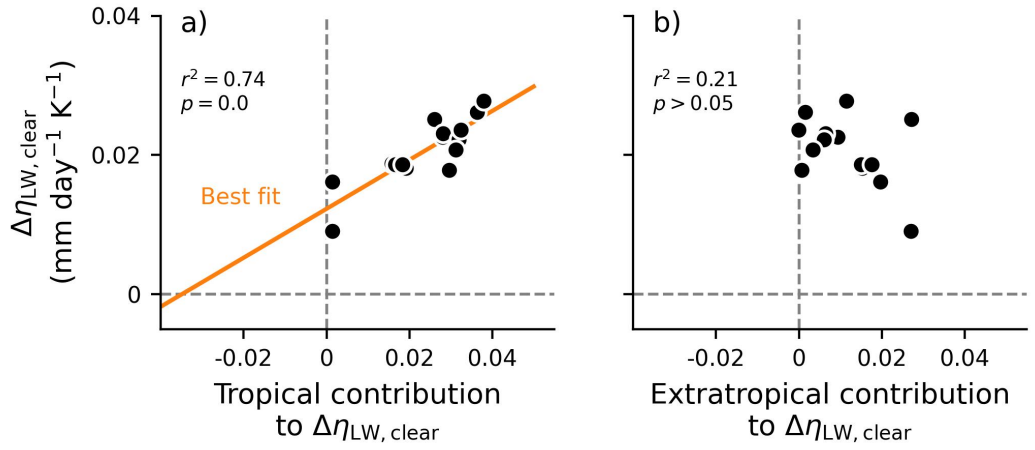

Figure 2. ***Differences in longwave clear-sky cooling between uniform and abrupt-4xCO_2 experiments are driven by changes in the tropics.*** (a) Scatterplot of $\Delta\eta_{\mathrm{LW,clear}}$ against the contribution from tropical changes in longwave, clear-sky cooling. (b) Scatterplot of $\Delta\eta_{\mathrm{LW,clear}}$ against the contribution from extratropical changes in longwave, clear-sky cooling.

Figure 2 shows that $\Delta\eta_{\mathrm{LW,clear}}$ is strongly correlated across models with the changes in tropical longwave, clear-sky cooling (Fig. 2a; $r^2 = 0.74$, $p < 0.01$), and not significantly correlated with extratropical changes in longwave, clear-sky cooling (Fig. 2b; $r^2 = 0.21$, $p > 0.05$). The small correlation with the extratropical contribution is entirely a result of the `IPSL-CM5A-LR` model, and the correlation reduces to $r^2 = 0.04$, $p = 0.46$ if this outlier is removed, while the correlations in Fig. 2a are largely unaffected.

Fitting a line of best fit to the data in Fig. 2a yields the following relationship between $\Delta\eta_{\mathrm{LW,clear}}$ and its tropical component, $\Delta\left\langle\eta_{\mathrm{LW,clear}}\right\rangle$:

$$\Delta\eta_{\mathrm{LW,clear}} \approx \alpha + \beta\,\Delta\left\langle\eta_{\mathrm{LW,clear}}\right\rangle. \tag{6}$$

The coefficients in Eq. 6 are $\alpha \approx 0.01$ mm day^{-1} K^{-1} and $\beta \approx 0.35$, but where do these values come from? Because the tropics and extratropics each cover $\frac{1}{2}$ of the Earth's surface we can write that $\eta = \frac{1}{2}(\eta^{\text{trop}} + \eta^{\text{extratrop}})$, where we have temporarily dropped the Δs and subscripts. This would imply a regression slope in Fig. 2a of $\frac{1}{2}$, and an intercept which is half the multi-model mean value of $\eta^{\text{extratrop}}$ (about ≈ 0.0055 mm day^{-1} K^{-1}). The reason that our best fit estimates of the slope (intercept) are biased high (low) compared to this is because there is a negative correlation between the tropical and extratropical contributions to $\Delta\eta_{\text{LW,clear}}$. This biases the slope to be somewhat smaller than 1/2, and because the slope and intercept of an ordinary least squares regression are inversely related, this also means that the intercept is biased high compared to our simple estimate. A short mathematical note to support this argument is provided in Supplemental Text S2.

Given these observations, for the rest of the paper we will mainly focus on understanding the *tropical* contribution to $\Delta\eta_{\text{LW,clear}}$, written as $\Delta\langle\eta_{\text{LW,clear}}\rangle$, and use Eq. 6 to convert this understanding to an estimate of the full $\Delta\eta_{\text{LW,clear}}$ when required.

5 A theoretical bridge between SST patterns and radiative cooling

We have shown that η is systematically larger in uniform warming experiments compared to abrupt-4xCO_2 forcing (a positive $\Delta\eta$), and that this is driven by the larger changes in longwave, clear-sky cooling ($\Delta\eta_{\text{LW,clear}}$) under uniform warming compared to abrupt-4xCO_2. In this section we develop a theory which links changes in clear-sky longwave cooling to SST patterns (building off the work of JR18) as a step towards explaining the positive $\Delta\eta_{\text{LW,clear}}$.

To begin with, we note that within the boundary layer radiative cooling is largely balanced by sensible heat fluxes, and so changes in clear-sky longwave cooling ($Q_{\text{LW,clear}}$) with warming can be approximated by changes in the longwave cooling of the *free-troposphere*, the area above the boundary layer but below the tropopause (see discussion in Takahashi (2009) and O'Gorman et al. (2012)). This allows us to leverage the work of Jeevanjee and Romps (2018), who developed a simple model of changes in *free-tropospheric* radiative cooling, to understand our results.

The theory of Jeevanjee and Romps (2018) starts from the observation that free-tropospheric radiative cooling can be written as the vertical integral of the radiative flux divergence in temperature coordinates ($-\partial_T F$, where ∂_T is a vertical derivative with respect to atmospheric temperature and F is the net upwards clear-sky radiative flux in the longwave). Mathematically, we write this as

$$Q_{\text{LW,clear}} \approx \int_{T_{\text{tp}}}^{T_{\text{LCL}}} (-\partial_{T'} F)\, dT', \tag{7}$$

where T_{tp} is the tropopause temperature and T_{LCL} is the temperature of the lifted condensation level (LCL), the lower boundary of the free-troposphere.

The utility of this perspective is that, based on simple radiative transfer theory, it can be shown that $-\partial_T F(T)$ depends only on the *local* atmospheric temperature, T, and does not depend on the temperature at any other level. Importantly, $-\partial_T F(T)$ is insensitive to changes in surface temperature, T_s. This 'T_s-invariance' arises because longwave radiative cooling is dominated by emission from optically-thick water vapor lines, which occur at a fixed atmospheric temperature (further discussion in Ingram (2010); Jeevanjee and Romps (2018)). Given that the tropopause temperature (T_{tp}) is also insensitive to surface temperature (Seeley et al., 2019; McKim et al., 2024), we can differentiate Eq. (7) to find the rate of change of $Q_{\text{LW,clear}}$ with respect to changes in surface temperature:

$$\frac{dQ_{\mathrm{LW,clear}}}{dT_s} \approx \left(-\partial_T F\right)|_{\mathrm{LCL}} \times \underbrace{\frac{dT_{\mathrm{LCL}}}{dT_s}}_{\text{Pattern effect}} . \tag{8}$$

In words, Eq. (6) says that surface warming increases Q_{FT} by an amount proportional to the value of the flux divergence at the LCL, and the derivative of LCL temperature with respect to surface temperature (dT_{LCL}/dT_s). Physically, this can be thought of as a 'deepening' of the troposphere in temperature coordinates (c.f. Figure 3 of Jeevanjee and Romps (2018)), which 'exposes' more of the $-\partial_T F(T)$ curve.

Jeevanjee and Romps (2018) showed that Eq. 8 held in uniform warming simulations, but neglected the dT_{LCL}/dT_s term by assuming that changes in T_{LCL} are equal to changes in T_s. Relaxing this final assumption is essential for understanding the link between SST patterns and changes in radiative cooling. For example, SST warming in the convective regions of the tropics is efficiently communicated to the whole of the tropical free-troposphere as a result of convective quasi-equilibrium and weak free-tropospheric temperature gradients (K. A. Emanuel et al., 1994; Fueglistaler et al., 2015; Y. Zhang & Fueglistaler, 2020; A. I. Williams et al., 2023). As a result, even though warming in tropical convective regions may constitute only a small change in global-mean SST, it generates a large change in global-/tropical-mean T_{LCL} through non-local warming of the free-troposphere. Hence, the pattern of SST warming can influence the change in free-tropospheric radiative cooling through altering the relationship between tropospheric and surface warming.

This theory (encapsulated in Eq. 8) precisely satisfies the goal set out in the introduction, namely to connect clear-sky radiative cooling to the SST pattern effect. A key implication of this theory is that, to the degree that models agree of the magnitude of $\left(-\partial_T F\right)|_{\mathrm{LCL}}$, we expect changes in dQ_{LW}/dT_s to scale with some measure of dT_{LCL}/dT_s across models, with the spread in dT_{LCL}/dT_s associated with different patterns of SST warming.

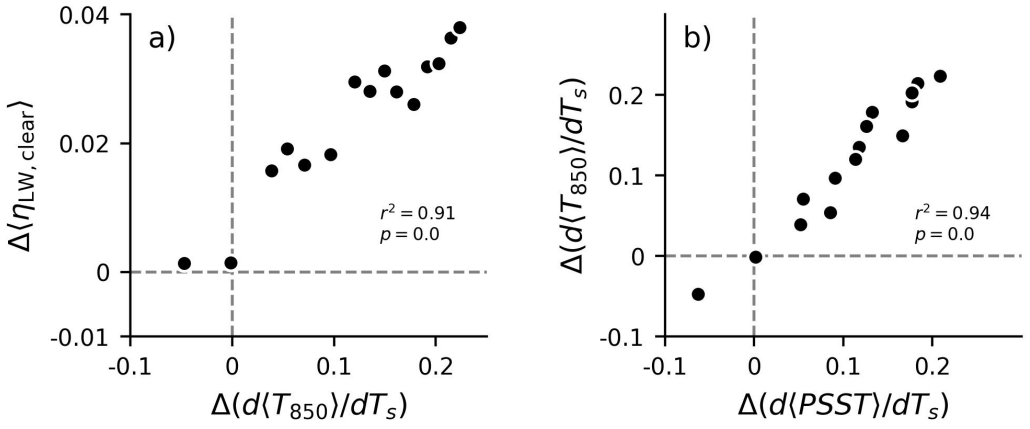

Figure 3. ***Changes in tropical, longwave clear-sky cooling are strongly correlated with the amount of warming in convective regions, as predicted by theory.*** (a) Scatterplot of $\Delta\langle\eta_{\mathrm{LW,clear}}\rangle$ against $\Delta\left(d\langle T_{850}\rangle/dT_s\right)$. (b) Scatterplot of $\Delta\left(d\langle T_{850}\rangle/dT_s\right)$ against $\Delta\left(d\langle \mathrm{PSST}\rangle/dT_s\right)$.

Given this, and recalling that we are interested in *tropical* longwave cooling (Figure 2a), we can use Eq. 8 to write the changes in tropical longwave cooling per degree of global warming ($\Delta \langle \eta_{\mathrm{LW,clear}} \rangle$) as

$$\Delta \langle \eta_{\mathrm{LW,clear}} \rangle \approx \langle -\partial_T F \rangle |_{\mathrm{LCL}} \times \Delta \left(\frac{d \langle T_{\mathrm{LCL}} \rangle}{dT_s} \right), \tag{9}$$

where $\frac{d\langle T_{\mathrm{LCL}} \rangle}{dT_s}$ is the change in tropical-mean LCL temperature per degree of global surface temperature change, Δ is the difference between a quantity calculated in uniform warming and abrupt-4xCO_2 simulations, and we have assumed that $\Delta \langle -\partial_T F \rangle |_{\mathrm{LCL}} = 0$.

To test Eq. 9, we approximate the temperature of the LCL by the temperature of the 850hPa pressure level (our results are qualitatively similar for other nearby pressure levels). In Fig. 3a we scatter $\Delta \langle \eta_{\mathrm{LW,clear}} \rangle$ against $\Delta \left(\frac{d\langle T_{\mathrm{LCL}} \rangle}{dT_s} \right)$ for each of the CMIP models. There is a strong, positive correlation between these two variables (r^2=0.92). Physically, this is saying that if a model has a large difference in $\frac{d\langle T_{\mathrm{LCL}} \rangle}{dT_s}$ between its uniform warming and abrupt-4xCO_2 experiments, then it will also have a large difference in the change in tropical, longwave clear-sky cooling per degree of global-warming, in line with our theory.

The slope of the linear relationship in Fig. 3a can also be interpreted as the multi-model mean value of $\langle -\partial_T F \rangle |_{\mathrm{LCL}}$. Converting to energy units, we find that the slope of the data implies a multi-model mean value of $\approx$ 3.8 W m^{-2} K^{-1}, which compares reasonably well with the $\langle -\partial_T F \rangle |_{850} \approx$ 3-4 W m^{-2} K^{-1} range of values diagnosed by JR18 using cloud-resolving simulations of tropical convection. This agreement gives us confidence that the 'tropospheric deepening' perspective is useful for explaining $\Delta \langle \eta_{\mathrm{LW,clear}} \rangle$.

Our theory is able to explain differences in tropical, clear-sky radiative cooling in terms of differences in $d \langle T_{850} \rangle / dT_s$, but now we would like to better understand what drives the spread in $\Delta \left(d \langle T_{850} \rangle / dT_s \right)$ across models. Physically, the temperature of the tropical free-troposphere is set by SSTs in regions of deep convection. This is because deep convection is the primary way in which the surface and the free-troposphere 'communicate' in the tropics (K. A. Emanuel et al., 1994; K. Emanuel, 2007; Sobel et al., 2001; Fueglistaler et al., 2015; A. I. Williams et al., 2023). It is thus natural to try and explain differences in $\Delta \left(d \langle T_{850} \rangle / dT_s \right)$ in terms of differences in the amount of SST warming which occurs in regions of tropical deep convection. To do this, in Fig. 3b we scatter $\Delta \left(d \langle T_{850} \rangle / dT_s \right)$ against changes in tropical, precipitation-weighted SST per degree of global-warming (written as $\Delta \left(d \langle \mathrm{PSST} \rangle / dT_s \right)$) (Flannaghan et al., 2014; Fueglistaler et al., 2015). The $\langle \mathrm{PSST} \rangle$ metric is calculated as $\langle P \cdot SST \rangle / \langle P \rangle$, where P is the precipitation and $\langle \cdot \rangle$ again denotes an area-weighted tropical average. PSST more strongly weights SST changes that occur in regions of deep convection with high precipitation, and thus captures the physical links between free-tropospheric temperatures, deep convection, and SSTs. As we can see in Fig. 3b, models which have a larger $d \langle T_{850} \rangle / dT_s$ in uniform warming than abrupt-4xCO_2 also exhibit greater SST warming in regions of tropical deep convection ($d \langle \mathrm{PSST} \rangle / dT_s$) under uniform warming than abrupt-4xCO_2 scenarios.

6 Tropical SST warming patterns drive $\Delta\eta$ across models

Now that we have developed a theory which links changes in tropical clear-sky longwave cooling to patterns of SST change, we return to the question of why $\eta_{\mathrm{LW,clear}}$ is systematically larger in uniform warming experiments than coupled experiments with abrupt-4xCO_2 forcing.

In Figure 4a, we show Gaussian distributions of $d \langle \mathrm{PSST} \rangle / dT_s$ in the ensemble of uniform warming and abrupt-4xCO_2 simulations. In abrupt-4xCO_2 simulations, $d \langle \mathrm{PSST} \rangle / dT_s$

is much more variable than in the uniform warming simulations, in line with the fact that the SST changes are identical in the uniform warming simulations, but model-dependent in the abrupt-4xCO_2 simulations. The salient feature of Figure 4a is that $d\langle \mathrm{PSST} \rangle / dT_s$ tends to be larger in uniform warming simulations than in abrupt-4xCO_2 simulations, reflecting the fact that warming in coupled models tends to be focused in the eastern tropical Pacific (sometimes referred to as being 'El Niño-like') where there is less convection and rainfall than in the western tropical Pacific. Meanwhile, uniform warming simulations warm SSTs over the deeply convecting regions of the tropics as much as the rest of the globe, thus generating a larger $d\langle \mathrm{PSST} \rangle / dT_s$.

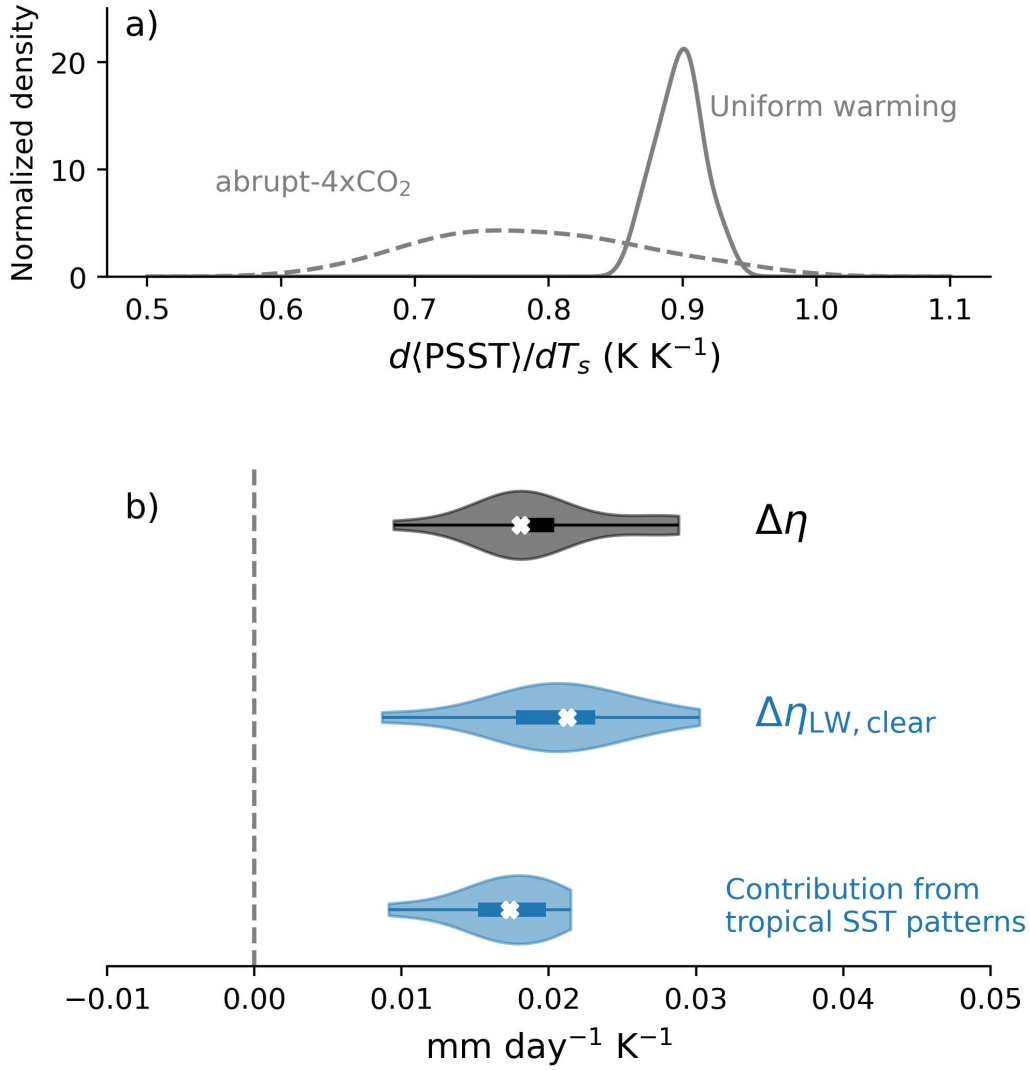

Figure 4. ***Differences in SST warming in convective regions largely account for differences in hydrological sensitivity.*** a) Kernel density estimates of changes in tropical PSST per degree of global warming in abrupt-4xCO_2 and uniform warming runs, The kernel density estimates are computed using the `gaussian_kde` function from SciPy (Virtanen et al., 2020). b) delta HS, LWCS contribution, and prediction of $\Delta\eta_{\mathrm{LW,clear}}$ using the differences in tropical precipitation-weighted SSTs across models.

To get a back-of-the-envelope estimate of how big an effect these inter-scenario differences in $d\langle \text{PSST} \rangle / dT_s$ have on tropical, longwave clear-sky cooling we can use Eq. 9 and replace $\langle T_{850} \rangle$ with $\langle \text{PSST} \rangle$,

$$\Delta \langle \eta_{\text{LW,clear}} \rangle \approx \langle -\partial_T F \rangle |_{\text{LCL}} \times \frac{d\langle \text{PSST} \rangle}{dT_s}. \tag{10}$$

The average $d\langle \text{PSST} \rangle / dT_s$ under uniform warming is ≈ 0.9 K K^{-1} compared to ≈ 0.78 K K^{-1} under abrupt-4xCO_2 forcing. Using these values in Eq. 10 along with a characteristic value of $\langle -\partial_T F \rangle |_{\text{LCL}} \approx 4$ W m^{-2} K^{-1} ≈ 0.14 mm day^{-1} K^{-1} yields a rough estimate of the change in tropical, longwave clear-sky cooling between uniform and abrupt warming scenarios of ≈ 0.017 mm day^{-1} K^{-1}. To convert this tropical estimate into an estimate of $\Delta\eta_{\text{LW,clear}}$, we use Eq. 6 (Fig. 2a). This yields an estimate of $\Delta\eta_{\text{LW,clear}} \approx 0.018$ mm day^{-1} K^{-1}, in good agreement with the average $\Delta\eta_{\text{LW,clear}}$ across the CMIP models (Fig. 4b).

We can use this procedure to estimate $\Delta\eta_{\text{LW,clear}}$ using $\Delta \left(d\langle \text{PSST} \rangle / dT_s \right)$ for each of the CMIP models, and the distribution of these estimates is also shown in Fig. 4b. This estimate relies only on our theory (Eq. 10), $d\langle \text{PSST} \rangle / dT_s$, and a small, empirical correction (Eq, 6) which relates tropical changes to global changes in longwave clear-sky cooling. The resulting distribution gives a reasonable estimate of $\Delta\eta_{\text{LW,clear}}$ across models, although slightly underestimates the high-end of changes. However, as we stated in Section 3, our goal here is to explain the multi-model mean value of $\Delta\eta$, which is closely-approximated by our estimate.

7 Conclusions

Our main results are:

- Hydrological sensitivity, η, is systematically larger in uniform warming than abrupt-4xCO_2 scenarios (Fig. 1a), associated with larger increases in longwave clear-sky radiative cooling in uniform warming runs (Fig. 1b).
- These differences in longwave, clear-sky cooling are driven by changes in longwave, clear-sky cooling in the tropics (Fig. 2a).
- These changes in longwave, clear-sky cooling are related to different SST warming rates in regions of tropical deep convection.
- Existing theories for radiative cooling and hydrological sensitivity can be extended to incorporate the SST pattern effect (Eq. 10).

This new understanding of the links between SST patterns and radiative cooling, encapsulated in Eq. 10, can be used to understand some of the intriguing results we referenced in the introduction. As a reminder, both Zhao and Knutson (2024) and S. Zhang et al. (2023) previously found that η was different depending on the pattern of SST warming, but neither provided a compelling physical argument for why this should be the case. Zhao and Knutson (2024) found that η was larger when the observed pattern of SST warming was imposed in a model compared to when the pattern was taken from the historical run of a coupled climate model. This can be understood in our framework as being due to a stronger $d\langle \text{PSST} \rangle / dT_s$ in response to the observed SST pattern, which warms more strongly in the Western tropical Pacific (a convective region) than the Eastern tropical Pacific (a largely non-convective region). Similarly, S. Zhang et al. (2023) noted that when 'patches' of SST warming were imposed in the Western tropical Pacific, the resulting η was larger. Hence, differential warming in regions of tropical convection, and the subsequently different amounts of 'tropospheric deepening' (JR18), can explain different values of η seen in previous literature.

We have shown that $\eta_{\mathrm{LW,clear}}$ is related to patterns of tropical sea-surface temperature change, and that inter-model spread in *this component* of η can be related to changes in SSTs in regions of tropical convection. Given this, it is natural to ask whether SST patterns play any role in setting the inter-model spread in η within a given scenario (e.g. abrupt-4xCO_2). S. Zhang et al. (2023) argue that this is the case, and that half of the inter-model spread in η under abrupt-4xCO_2 forcing can be ascribed to differences in SST patterns. However, as we show in Supplementary Figure S3, there is no significant correlation between η and $\eta_{\mathrm{LW,clear}}$ across CMIP5/6 models under abrupt-4xCO_2 forcing. Hence, even though SST patterns do explain a large portion of the variance of $\eta_{\mathrm{LW,clear}}$ under abrupt-4xCO_2 forcing, this does not mean that SST patterns are a constraint on the *total* hydrological sensitivity (η).

We also note that Kao and Pendergrass (2024) recently found that the value of η depended in abrupt-4xCO_2 simulations depended on the *timescale* over which it was calculated. That is, whether the regressions were taken over years 1–20, 21–150 or 151–1000 of LongRunMIP simulations (Rugenstein et al., 2019). This behavior is similar to the timescale-dependence of the feedback parameter, λ, in abrupt-4xCO_2 simulations, which has been linked to changes in the pattern of warming over time (Dong et al., 2020). Future work could examine whether the timescale-dependence of η is due to changes in longwave cooling and if so, whether these changes are due to a timescale-dependence of the amount of warming in tropical convective regions.

8 Open Research

Data supporting the conclusions in this article are archived at A. I. L. Williams (2025).

Acknowledgments

A.I.L. Williams acknowledges funding from the CIMES Postdoctoral Fellowship under award NA18OAR4320123 from the National Oceanic and Atmospheric Administration, U.S. Department of Commerce.

We are thankful to Jonathan Gregory, Adam Sokol, Tim Merlis, Donghyun Lee, and Shipeng Zhang for helpful discussions. A.I.L. Williams is grateful to Cleo Haussler-Williams for her unwavering support during the writing process.

References

Allen, M. R., & Ingram, W. J. (2002, September). Constraints on future changes in climate and the hydrologic cycle. *Nature*, *419*(6903), 228–232. Retrieved from `https://doi.org/10.1038/nature01092` doi: 10.1038/nature01092

Bloch-Johnson, J., Rugenstein, M. A., Alessi, M. J., Proistosescu, C., Zhao, M., Zhang, B., ... others (2024). The green's function model intercomparison project (gfmip) protocol. *Journal of Advances in Modeling Earth Systems*, *16*(2), e2023MS003700.

DeAngelis, A. M., Qu, X., Zelinka, M. D., & Hall, A. (2015). An observational radiative constraint on hydrologic cycle intensification. *Nature*, *528*(7581), 249–253.

Dong, Y., Armour, K. C., Zelinka, M. D., Proistosescu, C., Battisti, D. S., Zhou, C., & Andrews, T. (2020). Intermodel spread in the pattern effect and its contribution to climate sensitivity in cmip5 and cmip6 models. *Journal of Climate*, *33*(18), 7755–7775.

Dong, Y., Proistosescu, C., Armour, K. C., & Battisti, D. S. (2019, September). Attributing Historical and Future Evolution of Radiative Feedbacks to Re-

gional Warming Patterns using a Green's Function Approach: The Preeminence of the Western Pacific. *Journal of Climate*, *32*(17), 5471–5491. (Publisher: American Meteorological Society Section: Journal of Climate) doi: 10.1175/JCLI-D-18-0843.1

Emanuel, K. (2007). Quasi-equilibrium dynamics of the tropical atmosphere. *The Global Circulation of the Atmosphere*, *186*, 218. doi: 10.1515/9780691236919-009

Emanuel, K. A., David Neelin, J., & Bretherton, C. S. (1994). On large-scale circulations in convecting atmospheres. *Quarterly Journal of the Royal Meteorological Society*, *120*(519), 1111–1143. Retrieved 2022-03-16, from https://onlinelibrary.wiley.com/doi/abs/10.1002/qj.49712051902 doi: 10.1002/qj.49712051902

Flannaghan, T. J., Fueglistaler, S., Held, I. M., Po-Chedley, S., Wyman, B., & Zhao, M. (2014). Tropical temperature trends in atmospheric general circulation model simulations and the impact of uncertainties in observed ssts. *Journal of Geophysical Research: Atmospheres*, *119*(23), 13–327.

Fläschner, D., Mauritsen, T., & Stevens, B. (2016). Understanding the intermodel spread in global-mean hydrological sensitivity. *Journal of Climate*, *29*(2), 801 - 817. Retrieved from https://journals.ametsoc.org/view/journals/clim/29/2/jcli-d-15-0351.1.xml doi: 10.1175/JCLI-D-15-0351.1

Fueglistaler, S., Radley, C., & Held, I. M. (2015). The distribution of precipitation and the spread in tropical upper tropospheric temperature trends in cmip5/amip simulations. *Geophysical Research Letters*, *42*(14), 6000–6007.

Ingram, W. (2010). A very simple model for the water vapour feedback on climate change. *Quarterly Journal of the Royal Meteorological Society: A journal of the atmospheric sciences, applied meteorology and physical oceanography*, *136*(646), 30–40.

Jeevanjee, N., & Romps, D. M. (2018). Mean precipitation change from a deepening troposphere. *Proceedings of the National Academy of Sciences*, *115*(45), 11465–11470. doi: 10.1073/pnas.1720683115

Kao, K., & Pendergrass, A. G. (2024). Timescale dependence of the precipitation response to co2-induced warming in millennial-length climate simulations. *Geophysical Research Letters*, *51*(21), e2024GL111609.

Manabe, S., & Wetherald, R. T. (1975). The effects of doubling the co 2 concentration on the climate of a general circulation model. *Journal of Atmospheric Sciences*, *32*(1), 3–15.

McKim, B. A., Jeevanjee, N., Vallis, G. K., & Lewis, N. T. (2024). Water vapor spectroscopy and thermodynamics constrain earth's tropopause temperature. *Authorea Preprints*.

Mitchell, J., Wilson, C., & Cunnington, W. (1987). On co2 climate sensitivity and model dependence of results. *Quarterly Journal of the Royal Meteorological Society*, *113*(475), 293–322.

O'Gorman, P. A., Allan, R. P., Byrne, M. P., & Previdi, M. (2012). Energetic constraints on precipitation under climate change. *Surveys in geophysics*, *33*, 585–608.

Pendergrass, A. G., & Hartmann, D. L. (2014). The atmospheric energy constraint on global-mean precipitation change. *Journal of Climate*, *27*(2), 757 - 768. Retrieved from https://journals.ametsoc.org/view/journals/clim/27/2/jcli-d-13-00163.1.xml doi: 10.1175/JCLI-D-13-00163.1

Qin, Y., Zelinka, M. D., & Klein, S. A. (2022). On the correspondence between atmosphere-only and coupled simulations for radiative feedbacks and forcing from co2. *Journal of Geophysical Research: Atmospheres*, *127*(3), e2021JD035460.

Rugenstein, M., Bloch-Johnson, J., Abe-Ouchi, A., Andrews, T., Beyerle, U., Cao, L., ... others (2019). Longrunmip: motivation and design for a large collection

of millennial-length aogcm simulations. *Bulletin of the American Meteorological Society*, *100*(12), 2551–2570.

Seeley, J. T., Jeevanjee, N., & Romps, D. M. (2019). Fat or fitt: Are anvil clouds or the tropopause temperature invariant? *Geophysical Research Letters*, *46*(3), 1842–1850.

Sobel, A. H., Nilsson, J., & Polvani, L. M. (2001, December). The Weak Temperature Gradient Approximation and Balanced Tropical Moisture Waves. *Journal of the Atmospheric Sciences*, *58*(23), 3650–3665. Retrieved 2022-03-16, from `https://journals.ametsoc.org/view/journals/atsc/58/23/1520-0469_2001_058_3650_twtgaa_2.0.co_2.xml` (Publisher: American Meteorological Society Section: Journal of the Atmospheric Sciences) doi: 10.1175/1520-0469(2001)058⟨3650:TWTGAA⟩2.0.CO;2

Takahashi, K. (2009). Radiative constraints on the hydrological cycle in an idealized radiative–convective equilibrium model. *Journal of the atmospheric sciences*, *66*(1), 77–91.

Virtanen, P., Gommers, R., Oliphant, T. E., Haberland, M., Reddy, T., Cournapeau, D., ... others (2020). Scipy 1.0: fundamental algorithms for scientific computing in python. *Nature methods*, *17*(3), 261–272.

Voigt, A., North, S., Gasparini, B., & Ham, S.-H. (2024). Atmospheric cloud-radiative heating in cmip6 and observations and its response to surface warming. *Atmospheric Chemistry and Physics*, *24*(17), 9749–9775.

Williams, A. I., Jeevanjee, N., & Bloch-Johnson, J. (2023). Circus tents, convective thresholds, and the non-linear climate response to tropical ssts. *Geophysical Research Letters*, *50*(6), e2022GL101499.

Williams, A. I. L. (2025). Supporting data for "sea-surface temperature patterns, radiative cooling, and hydrological sensitivity". [dataset]. *Zenodo*. doi: https://doi.org/10.5281/zenodo.15733243

Zhang, B., Zhao, M., & Tan, Z. (2023). Using a green's function approach to diagnose the pattern effect in gfdl am4 and cm4. *Journal of Climate*, *36*(4), 1105–1124. doi: 10.1175/JCLI-D-22-0024.1

Zhang, S., Stier, P., Dagan, G., Zhou, C., & Wang, M. (2023). Sea surface warming patterns drive hydrological sensitivity uncertainties. *Nature Climate Change*, *13*(6), 545–553.

Zhang, Y., & Fueglistaler, S. (2020). How Tropical Convection Couples High Moist Static Energy Over Land and Ocean. *Geophysical Research Letters*, *47*(2), e2019GL086387. Retrieved 2022-03-16, from `https://onlinelibrary.wiley.com/doi/abs/10.1029/2019GL086387` doi: 10.1029/2019GL086387

Zhao, M., & Knutson, T. (2024). Crucial role of sea surface temperature warming patterns in near-term high-impact weather and climate projection. *npj Climate and Atmospheric Science*, *7*(1), 130.

Zhou, C., Zelinka, M. D., & Klein, S. A. (2017). Analyzing the dependence of global cloud feedback on the spatial pattern of sea surface temperature change with a Green's function approach. *Journal of Advances in Modeling Earth Systems*, *9*(5), 2174–2189. doi: 10.1002/2017MS001096